Physica B 639 (2022) 413991

Contents lists available at ScienceDirect

Physica B: Physics of Condensed Matter

journal homepage: www.elsevier.com/locate/physb

Evaluation of the external electric- and magnetic field-driven Mathieu quantum dot's optical observables

P. Başer *, M.K. Bahar

Department of Physics, Faculty of Science, Sivas Cumhuriyet University, 58140, Sivas, Turkey

ARTICLE INFO

Keywords:
Nonlinear optical properties
Quantum dot
Mathieu potential
Electric field
Magnetic field

ABSTRACT

In this study, for the first time, the total refractive index changes (TRICs) and total absorption coefficients (TACs) of the quantum dot including the Mathieu potential confinement formed by the $In_xGa_{1-x}As/GaAs$ heterostructure under the influence of external electric and magnetic fields are theoretically investigated. The spectra and eigenfunctions of the Mathieu quantum dot are obtained using the effective mass approximation by forming a tridiagonal matrix formalism. The iterative method and compact-density-matrix formalism are used together to examine the nonlinear optical properties of the Mathieu quantum dot. Throughout the study, the effects on the TRICs and TACs of the external electric and magnetic field, as well as the In concentration and confinement width, are probed. Considering the strong and weak regimes of the external electric and magnetic fields, their alternatives to the structural parameters in terms of optical properties are also evaluated. The increment of the In concentration causes the quantum dot encompassment to turn into the opposite character after a certain radial distance. This result may be remarkable in terms of experimental applications. Under certain conditions, the incident optical intensities photons on the structure are determined at the limit values. As well as determining the functional range of the Mathieu quantum dot in terms of the TRICs and TACs characters, using both structure parameters and external fields and as a function of the incident photon energy, the determination of the optimum for these characters is an important theoretical gain in terms of providing a prediction for experimental studies.

1. Introduction

Semiconductor quantum dots provide an almost ideal zero-dimensional quantum confinement for charge carriers. These structures are also called artificial atomic structures because of their atom-like energy states. They have a sharper density of states compared to three-dimensional confinement effects, quantum wires and two-dimensional quantum wells. Therefore, they have superior handling and optical properties. Electronic devices including these structures can operate faster as the confinement effects force particles to move in a very small volume. Due to their three-dimensional confinement effects, quantum dots have a sharper state density than quantum wires, which have two-dimensional confinement, and quantum wells, which have one-dimensional confinement. Therefore, they have more widely usage areas and more unique optical properties compared to other low-dimensional systems. Due to the aforementioned properties, quantum dots are used extensively in the construction of many opto-electronic devices such as quantum dot solar cells [1–3], quantum dot lasers [4,5], quantum dot photodetectors [6–8] and quantum dot infrared photodetectors [9], phototransistors [10] and light emitting diodes [11–13]. Optoelectronic device applications have received a lot of attention in recent years. It is important to note that $In_xGa_{1-x}As/GaAs$ quantum dots obtained by growing group III-V materials show interesting properties in optoelectronic and microelectronic applications [14–17]. Also, InGaAs triple alloys are among the most important semiconductor materials used in the electro-optical systems [18]. These alloys have a major role on the development of high-powered electronical and optoelectronical devices. Comparing to other known semiconductors such as gallium arsenic and silicon, the particles in this semiconductor move at very high speeds and the femtosecond lifetime of the carriers makes them superior in device designs. When the In concentration of the semiconductor compound of InGaAs is changed in the range of $x = 0 - 1$, the band gap of InGaAs changes from 0.36 to 1.42 eV. This wide bandwidth of InGaAs makes it advantageous to employ in detector and fiber optic technology [19]. High speed optoelectronic devices such as photodetectors, high electron mobility transistors, photodiodes, metal semiconductor, metal photodetectors, multiplet lasers, infrared lasers can be obtained by employing InGaAs compound [20–25].

* Corresponding author.
E-mail addresses: pbaser34@gmail.com (P. Başer), mussiv58@gmail.com (M.K. Bahar).

https://doi.org/10.1016/j.physb.2022.413991
Received 2 March 2022; Received in revised form 6 April 2022; Accepted 2 May 2022
Available online 11 May 2022

The effects of an external electric and magnetic field on the electronic properties of quantum dots cause to considerable theoretical and experimental results. Because, external fields change the energy levels of the electron by providing an extra confinement effect on the particles. In addition, it is also reality that the carrier lifetimes vary depending on the external fields [26–30]. The electric field applied to the $In_xGa_{1-x}As/GaAs$ quantum dots changes the probability of trapping electrons. These observations can be explained by the increase in the velocity of the charges confined in the quantum dots. That is, the electric field increases the trapping of particles in quantum dots and causes a factor of five increase in emitted light [31]. Under the influence of an external magnetic field, significant informations can be obtained about the electronic and structural properties of quantum dot. We can divide the effects arising from the magnetic field into two classes: Firstly, one of the features that the magnetic field acting to the structure is the change of direction of the carrier motion and the formation of Landau levels. If a charged particle moves perpendicular to an applied magnetic field, its orbit bends. The force acting on the particle, namely the Lorenz force, is perpendicular to both the magnetic field and the particle velocity, and if the magnetic field is sufficiently strong compared to other scattering processes (such as particle–particle collisions), the particle orbit becomes circular. Thus, the external magnetic field applied on the quantum dots will create an extra confinement effect on the particle in the plane perpendicular to the magnetic field. As the magnetic field increases, a diamagnetic shift in energy levels occurs. Deflection of charged particles by the magnetic field can be used as an implement in tuning carrier density in quantum dots. This provides a very influential factor in device designs [32]. Secondly, due to the magnetic field, the separation occurs in the energy levels of the particle which has different angular momentum and different spin values. This effect, which is well known in the literature, is called the Zeeman effect. Similar to the Zeeman effect, the separation in the energy levels of electrons in a quantum dot arising from the magnetic field is called as the Fock Darwin spectrum [33–35]. External electric and magnetic fields applied on the structure change the electronic structure by creating extra confinement effects and then, change the non-linear optical effects. Zhang et al. have studied the effects of external fields on the TRICs and TACs of the parabolic quantum dot. They have showed that the external fields make significant changes in the linear absorption coefficient and refractive index, as the applied electric field and magnetic field change the confinement effects [36]. On the other hand, Monica et al. have investigated the linear and third-order nonlinear optical properties of an exciton confined to a three-dimensional quantum dot with a parabolic potential under a static magnetic field. They have showed that as the trapping effect of the electron under the magnetic field increases, the spatial separation between the electron and the hole increases, thus the energy separation of the quantum system increases, and then causing blueshifted the absorption curves [37]. Sargsian et al. have studied theoretically the linear and third-order nonlinear absorption coefficients and refractive index in the cylindrical quantum dot with the Morse and modified Pöschl-Teller potential under external electric and magnetic fields [38]. In this study, both the direction and strength of the electric field have been considered. The increment of the electric field leads to a redshift in the resonant frequencies of TRICs and TACs, while an electric field in the opposite direction shifts them to blue. The study of the optical properties of a hydrogenic impurity at the center of an azimuthal distortion quantum disk is a very current topic, and the multifunctional properties of the distortion on TRICs and TACs have been identified [39]. It should be pointed out that external fields cause significant changes not only on the TRICs and TACs but also optical observables such as second harmonic generation [40], third harmonic generation [41], and nonlinear optical correction [42].

For the best of the our knowledge, the Mathieu potential as the quantum dot encompassment potential is taken into consideration theoretically in the present study in the related literature, for the first time. Mathieu functions play an important role in many different fields of physics or in practical applications. Some of these applications can be exemplified as solution of the quantum mechanical problem of the rotation of molecules by regarding the Mathieu potential [43], the cosine potential application to the scattering theory [44], investigation of the phase space properties by using the Mathieu potential [45], new electron states of hydrogen subjected to a circularly polarized electromagnetic manipulated by the parameters of Mathieu functions [46]. This potential having the parabolic quantum structure, can be obtained by growth techniques and the respective calculations can be adapted device designs. In the present study, polar coordinates are more suitable for the symmetry of the system due to the applied magnetic field in the z-direction. So, polar coordinates are considered in the study and essentially the system is a $2D$ quantum dot. In this study, the effects of the structural parameters such as the quantum dot radius, the potential depth and the external fields such as the electric field and magnetic field on electronic energies, the total absorption coefficients (TACs) and the total refractive index changes (TRICs) are investigated. Therefore, we aim to determine optimum conditions for the quantum dot with Mathieu confinement potential in consideration of TRICs and TACs to obtain useful data in possible technological applications of such quantum dots.

The article is organized as follows: Section 2 describes the theoretical model used in the work. In Section 3, the results obtained, and their comments are presented. In Section 4, the crucial outcomes are outlined.

2. Theoretical model

The Hamiltonian for the Mathieu quantum dot system, produced by the InGaAs/GaAs heterostructure, under the influence of the external electric and magnetic field is written as

$$H = \frac{1}{2m^\star}(\vec{\mathbf{P}} - e\mathbf{A}(\vec{\mathbf{r}}))^2 + V_{dot}(r) + e\mathbf{F}.\mathbf{r} \tag{1}$$

where, e is the electron charge, $m^\star$ is the effective mass of the electron, F is the external electric field strength, and $V_{dot}(r)$ is the Mathieu quantum dot confinement potential. The Mathieu confinement potential is given by [47]

$$V_{dot}(r) = V_0[\sin^2(\eta r) - \cos(\eta r)], \tag{2}$$

where V_0 is the potential depth parameter, changes depending on In−concentration (being x In−concentration) as $V_0 = (1.42 - 1.53x + 0.45x^2)$ eV [48], η is the potential width parameter. If the gauge of the $\vec{A} = (1/2)(\vec{B} \times \vec{r})$ for the vector potential is employed, and taken into consideration the direction as $B_x = B_y = 0$ and $B_z = B$ for the components of the external magnetic field (B), the Hamiltonian is converted to

$$H = -\frac{\hbar^2\nabla^2}{2m^\star} + \frac{m^\star\omega_c^2}{8}(x^2 + y^2) + \frac{\omega_c}{2}L_z + V_{dot}(r) + eFr, \tag{3}$$

where, as can be seen, the external electric field is parallel to the radial direction. Also, as well-known, ω_c is the cyclotron frequency in crystals, and it is given by $\omega_c = eB/m^\star$ [49]. Under these conditions, the wave equation to be solved is $H\Phi(\mathbf{r}) = E\Phi(\mathbf{r})$. However, the symmetry of the quantum system is appropriate for the polar coordinates (r, ϕ). When considering the polar coordinates as $x = r\cos\phi$ and $y = r\sin\phi$, and employing the following transformation, being m the magnetic quantum number,

$$\Phi_{nm}(\mathbf{r}) = \frac{e^{im\phi}}{\sqrt{2\pi}}\frac{\psi(r)}{\sqrt{r}}, \tag{4}$$

the relevant wave equation becomes the radial second-order differential equation as follows

$$\frac{d^2\psi(r)}{dr^2} + \frac{2m^\star}{\hbar^2}\left[E_{nm} - V_{eff}(r)\right]\psi(r) = 0. \tag{5}$$

In this radial differential equation, $V_{eff}(r)$ is the effective potential of the Mathieu quantum dot system, and given by

$$V_{eff}(r) = \frac{m\hbar\omega_c}{2} + \frac{(m^2-(1/4))\hbar^2}{2m^\star r^2} + \frac{m^\star\omega_c^2}{8}(r^2) + V_{dot}(r) + eFr. \quad (6)$$

Ultimately, the wave equation needs to be solved in order to examine the electronic and optical properties. For this, the tridiagonal method, which is a numerical method, is preferred in the present study. The tridiagonal matrix method is employed to obtain the solutions of the eigenvalue equation $H\Phi(\mathbf{r}) = E\Phi(\mathbf{r})$ [50]. This method bases the Taylor series to discrete derivative expression of the eigenfunctions as $\psi'' = [(\psi(r+\delta)-2\psi(r)+\psi(r-\delta))/\delta^2]+O(\delta^2)$, where $\delta = (r_{max}-r_{min})/n_{step}$ when taken into considering r_i $(i = 0, 1, 2, \ldots, n_{step})$. n_{step} is the step number. By considering ψ'' expression, the diagonal and nondiagonal matrix elements are found. The eigenvalue equation of the system is constituted in a different form by utilizing all matrix elements. This form involves a tridiagonal matrix with (1000×1000) dimension. For details of the method, please refer [50].

After obtaining the bound state energies and associated wave functions of the Mathieu quantum dot, nonlinear optical properties can be studied. When acting a linearly polarized electromagnetic field containing ω frequency on the Mathieu quantum dot, and the time-dependent electromagnetic field is expressed as [51]

$$E(t) = E_0\cos(\omega t) = \tilde{E}e^{i\omega t} + \tilde{E}e^{-i\omega t} \quad (7)$$

Being V, σ and ε_0 are the system volume, the one-electron density-matrix of the system, the dielectric constant of vacuum, if the electronic polarization $P(t)$ and susceptibility $\chi(t)$ are introduced through the dipole operator M in the following form:

$$P(t) = \varepsilon_0\chi(\omega)\tilde{E}e^{-i\omega t} + \varepsilon_0\chi(-\omega)\tilde{E}e^{i\omega t} = \frac{1}{V}Tr(\sigma M). \quad (8)$$

The linear and nonlinear susceptibilities are specified by employing same density-matrix formalism, and then the respective closed analytical statements are stated as

$$\varepsilon_0\chi^{(1)}(\omega) = \frac{(\frac{m^\star k_B T}{\pi\hbar^2 R_{dot}} In[\frac{1+exp[(E_F-E_{min})/k_BT]}{1+exp[(E_F-E_{max})/k_BT]}])|M_{fi}|^2}{E_{fi}-\hbar\omega-i\hbar\Gamma_{if}}, \quad (9)$$

$$\begin{aligned}\varepsilon_0\chi^{(3)}(\omega) = & -\frac{(\frac{m^\star k_B T R_{dot}}{\pi\hbar^2} In[\frac{1+exp[(E_F-E_{min})/k_BT]}{1+exp[(E_F-E_{max})/k_BT]}])|M_{fi}|^2|\tilde{E}|^2}{E_{fi}-\hbar\omega-i\hbar\Gamma_{if}} \\ & \times [\frac{4|M_{fi}|^2}{(E_{fi}-\hbar\omega)^2+(\hbar\Gamma_{if})^2} - \\ & \frac{(M_{ff}-M_{ii})^2}{(E_{fi}-i\hbar\Gamma_{if})(E_{fi}-\hbar\omega-i\hbar\Gamma_{if})}], \end{aligned} \quad (10)$$

where k_B is the Boltzmann constant, E_F is the Fermi energy level, T is the temperature, E_{min} and E_{max} are, respectively, the subband minima and maxima [49], $E_{i,f}$ is the initial (i) and final (f) energy state, M_{fi} is the dipole matrix elements designated by $M_{fi} = \langle f|er|i\rangle$ where f is the final state, and i is the initial state, $\Gamma = 1/\tau$ is the relaxation rate for i, f states. Then, being n_r the refractive index, the refractive index change is introduced as,

$$\frac{\Delta n(\omega)}{n_r} = Re(\frac{\chi(\omega)}{2n_r^2}). \quad (11)$$

Considering Eqs. (9)–(11), the linear and the third-order nonlinear RICs are procured by [51,52].

$$\begin{aligned}\frac{\Delta n^{(1)}(\omega)}{n_r} = & \frac{(\frac{m^\star k_B T}{\pi\hbar^2 R_{dot}} In[\frac{1+exp[(E_F-E_{min})/k_BT]}{1+exp[(E_F-E_{max})/k_BT]}])|M_{fi}|^2}{2n_r^2\varepsilon_0} \\ & [\frac{E_{fi}-\hbar\omega}{(E_{fi}-\hbar\omega)^2+(\hbar\Gamma_{if})^2}], \end{aligned} \quad (12)$$

$$\begin{aligned}\frac{\Delta n^{(3)}(\omega,I)}{n_r} = & -\frac{\mu c|M_{fi}|^2}{4n_r^3\varepsilon_0}\frac{(\frac{m^\star k_B T}{\pi\hbar^2 R_{dot}} In[\frac{1+exp[(E_F-E_{min})/k_BT]}{1+exp[(E_F-E_{max})/k_BT]}])I}{[(E_{fi}-\hbar\omega)^2+(\hbar\Gamma_{if})^2]^2} \\ & \times[4(E_{fi}-\hbar\omega)|M_{fi}|^2 - \frac{(M_{ff}-M_{ii})^2}{(E_{fi})^2+(\hbar\Gamma_{if})^2}\{(E_{fi}-\hbar\omega) \\ & \times[(E_{fi})(E_{fi}-\hbar\omega)-(\hbar\Gamma_{if})^2]-(\hbar\Gamma_{if})^2(2(E_{fi})-\hbar\omega)\}], \end{aligned} \quad (13)$$

where being μ, c are, respectively, the permeability of the system, the velocity of light in vacuum, I as the incident optical intensity is defined by the following form

$$I = 2\sqrt{\frac{\varepsilon_R}{\mu}}|E(\omega)|^2 = \frac{2n_r}{\mu c}|E(\omega)|^2, \quad (14)$$

where ε_R the real part of the permittivity. The TRIC is figure out by considering the linear and nonlinear contributions [51]:

$$\frac{\Delta n(\omega,I)}{n_r} = \frac{\Delta n^{(1)}(\omega)}{n_r} + \frac{\Delta n^{(3)}(\omega,I)}{n_r}. \quad (15)$$

However, the AC change is expressed by

$$\alpha(\omega) = \omega(\frac{\mu}{\varepsilon_R})^{1/2} Im(\varepsilon_0\chi(\omega)), \quad (16)$$

where $\chi(\omega)$ is the Fourier component of $\chi(t)$. The linear and the third-order nonlinear ACs are procured by

$$\alpha^{(1)}(\omega) = \omega\sqrt{\frac{\mu}{\varepsilon_r}}\frac{|M_{fi}|^2(\frac{m^\star k_B T}{\pi\hbar^2 R_{dot}} In[\frac{1+exp[(E_F-E_{min})/k_BT]}{1+exp[(E_F-E_{max})/k_BT]}])\hbar\Gamma_{if}}{(E_{fi}-\hbar\omega)^2+(\hbar\Gamma_{if})^2}, \quad (17)$$

$$\begin{aligned}\alpha^{(3)}(\omega,I) = & -2\omega\sqrt{\frac{\mu}{\varepsilon_R}}(\frac{I}{\varepsilon_0 n_r c}) \\ & \times \frac{|M_{fi}|^4(\frac{m^\star k_B T}{\pi\hbar^2 R_{dot}} In[\frac{1+exp[(E_F-E_{min})/k_BT]}{1+exp[(E_F-E_{max})/k_BT]}])\hbar\Gamma_{if}}{[(E_{fi}-\hbar\omega)^2+(\hbar\Gamma_{if})^2]^2} \\ & (1-\frac{|M_{ff}-M_{ii}|^2}{|2M_{fi}|^2} \\ & \times \frac{(E_{fi}-\hbar\omega)^2-(\hbar\Gamma_{01})^2+2(E_{fi})(E_{fi}-\hbar\omega)}{(E_{fi})^2+(\hbar\Gamma_{if})^2}). \end{aligned} \quad (18)$$

The TAC is represented by evaluating the linear and nonlinear contributions [51]:

$$\alpha(\omega,I) = \alpha^{(1)}(\omega) + \alpha^{(3)}(\omega,I). \quad (19)$$

3. Result and discussions

In the InGaAs/GaAs Mathieu quantum dot structure, the variations of the external electric field, the magnetic field, the In concentration and the potential width have been investigated. Then, the effects of these variable parameters on the difference between the energy levels and on the matrix elements have been examined. Finally, as a function of the incident photon energy, the TRICs and TACs have been analyzed versus the change of the structure parameters and the external field strengths. Throughout the study, the quantum dot radius (R_{dot}) is taken as $6a_0$. The parameters used for GaAs structure in the calculations are as follows: $\varepsilon = 13.18$ (the dielectric constant), $I = 0.1\times10^{10}\mathrm{W}/m^2$ (the incident optical intensity) $V_0 = 66.55$meV $(x = 0.25)$ (the confinement potential's depth), $\tau = 0.2$ps (the relaxation times). For GaAs, the effective Rydberg constant is $R_y = 5.28$meV ($R_y = 4.18$meV for $In_{0.25}Ga_{0.75}As$), while the effective Bohr radius is $a_0 = 103.83$ ∀ ($a_0 = 127.59$ ∀ for $In_{0.25}Ga_{0.75}As$). Throughout the study, the magnetic quantum number is taken as $m = 0$.

In Fig. 1, the effective potential given by Eq. (6) includes the Mathieu quantum dot potential, in which panel (a) is for the electric field strength (F), panel (b) is for the magnetic field strength (B), panel (c) is for the In concentration (x), panel (d) is for the Mathieu quantum dot's width (η). The effective potential profiles are presented as a function of the radial distance r depending on the change values of the respective parameters. The bound state wave functions shown on the potential profiles belong to the respective profile line, and

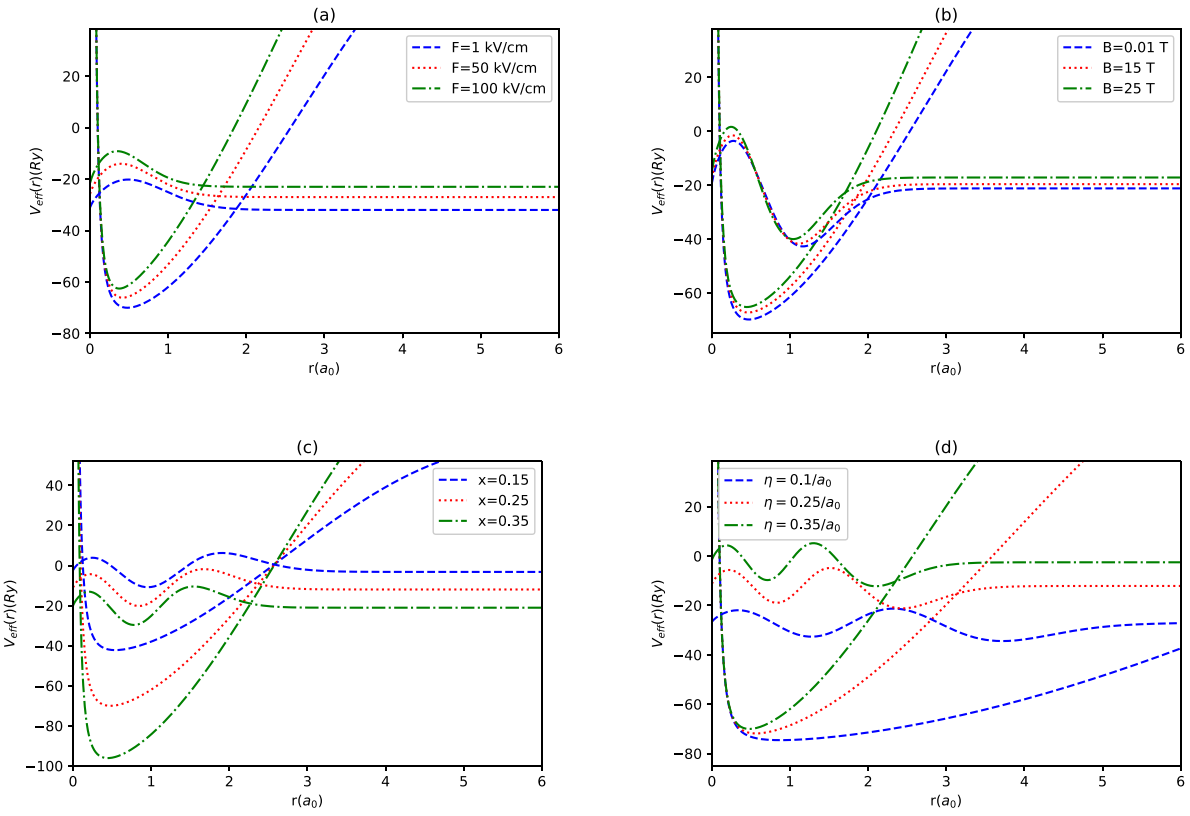

Fig. 1. The effective potential profile and the relevant wave functions of the Mathieu quantum dot system under the external electric and magnetic field for (a) $F = 1, 50, 100$ kV/cm when $B = 1$ T, $x = 0.25$ and $\eta = 0.35/a_0$, (b) $B = 0.01, 15, 25\ T$ when $F = 5$ kV/cm, $x = 0.25$ and $\eta = 0.35/a_0$, (c) $x = 0.15, 0.25, 0.35, 0.45$ when $F = 1$ kV/cm, $B = 1\ T$ and $\eta = 0.35/a_0$, (d) $\eta = 0.1, 0.25, 0.35/a_0$ when $F = 1$ kV/cm, $B = 1\ T$ and $x = 0.25$, in effective Rydberg units. Note: Same color wave functions and potential profiles are synchronized with each other.

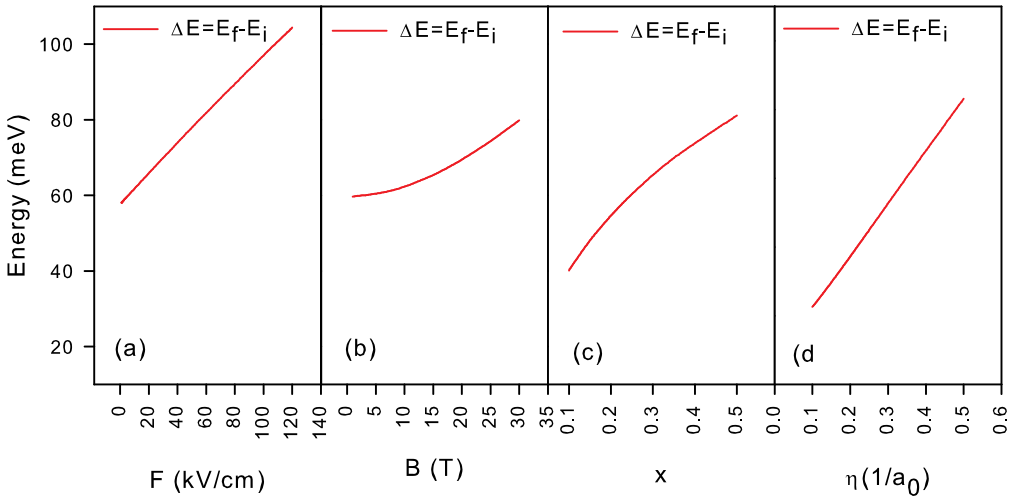

Fig. 2. The difference between the energy levels as a function of (a) F, (b) B, (c) x and (d) η parameters. The parameter set of each graph is synchronized with that of the TRICs and TACs graphs.

the corresponding energy level on the potential axis belongs to the respective wave function. As seen, the changes in the repulsiveness and attractiveness of the effective potential profile and the localizations of the wave functions are in very good agreement. In Fig. 2, we furnish the difference between the energy levels, as the $\Delta E = E_f - E_i$ (E_i:the ground state energy, E_f:the first excited state energy), of the Mathieu quantum dot as a function of F, B, x and η. It should be pointed out that there is a very good agreement between the observables in Fig. 2 and the potential interactions in Fig. 1. The examination of the behavior of the effective potential profile through these external fields and structure parameters is important in examining the external fields and structure parameters on the TRICs and TACs. In Fig. 3, the variation of matrix elements as a function of the same external fields and structure parameters mentioned is examined, as $|M_{fi}|^2$ and $|M_{ff} - M_{ii}|^2$. The matrix elements can change depending on the external parameters and the localizations of the energy levels (See Figs. 2 and 3). The matrix elements in Fig. 3a and 3b decrease with increasing electric and magnetic field. As a result, the probability of electron tunneling can be reduced or increased depending on the direction of the applied electric field. This controlling mechanism over tunneling can be used

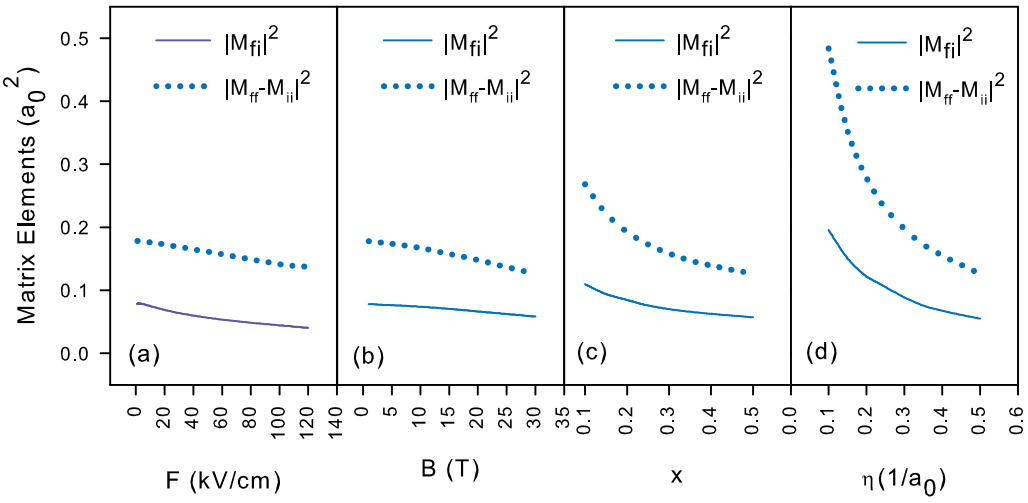

Fig. 3. The matrix elements as a function of (a) F, (b) B, (c) x and (d) η parameters. The parameter set of each graph is synchronized with that of the TRICs and TACs graphs.

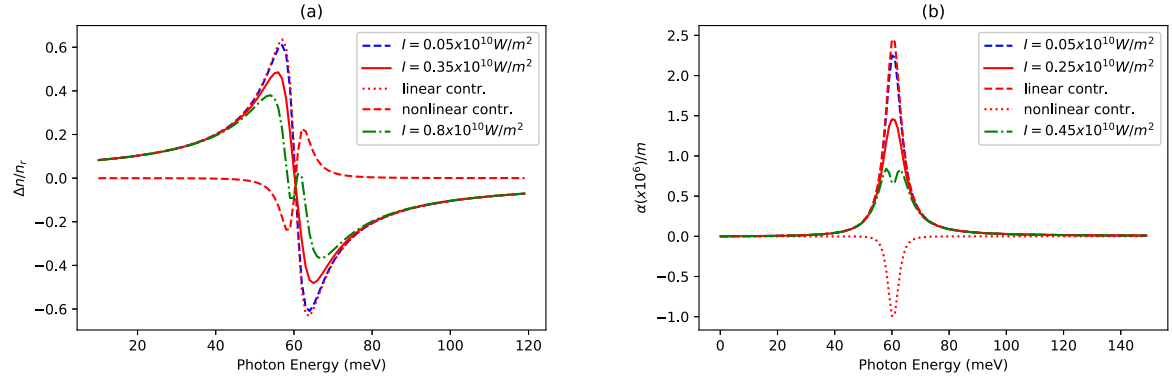

Fig. 4. When considering the different $I-$ values, the change of (a) the TRICs and (b) TACs of the Mathieu quantum dot with $x = 0.25$ and $\eta = 0.35$ under the effect of the external electric ($F = 5$ kV/cm) and magnetic field ($B = 5$ T), as a function of the incident photon energy. The linear and nonlinear contributions (red lines) in the TRICs characteristic are shown for only $I = 0.35 \times 10^{10}$ W/m^2, whereas ones (red lines) in the TACs characteristic are shown for only $I = 0.25 \times 10^{10}$ W/m^2. (For interpretation of the references to color in this figure legend, the reader is referred to the web version of this article.)

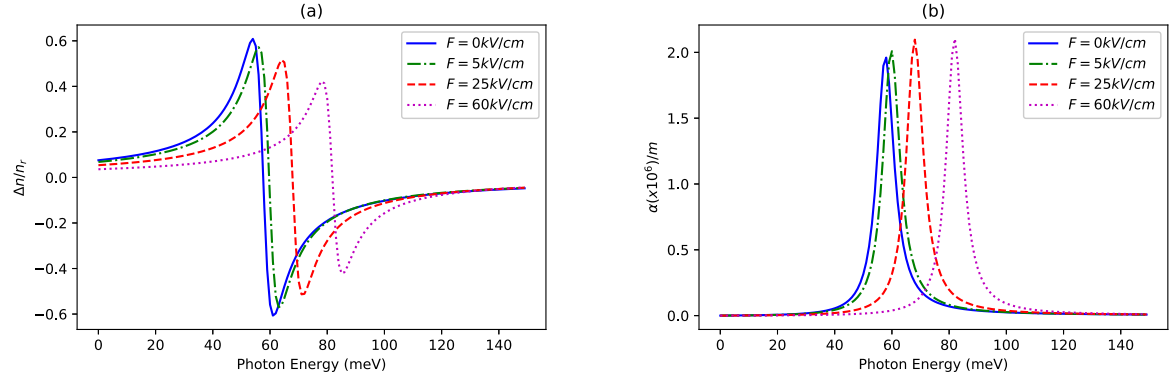

Fig. 5. (a) The TRICs and (b) TACs of the Mathieu quantum dot with $V_0 = 215.29$ meV ($x = 0.25$) and $\eta = 0.35/a_0$, under the influence of the external electric ($F = 5 - 25 - 60 - 100$ kV/cm) and magnetic field ($B = 1$ T), as a function of the incident photon energy.

for a variety of device applications such as photodetectors and high-power field effect transistors. In Fig. 3c, it is seen that the matrix elements ($|M_{fi}|^2$) decrease as x increases, that is, as the potential depth increases, the matrix elements also decrease. The reason of this phenomenon is that the wave functions and their overlapping region become the extended region as V_0 decreases. Meanwhile, increasing x leads to the stronger effect of the confinement potential on the electronic states. Therefore, as the difference between the bound state energies increases with the increase of x, the matrix elements also decrease. Increasing the η parameter increases the energy difference between the ground and the first excited states, due to the increment of the repulsiveness of the quantum dot potential, as can be seen from Fig. 1d. As a result, it is seen in Fig. 3d that the $|M_{fi}|^2$ matrix elements decrease as the η parameter increases.

In Fig. 4, the optical intensity on the TRICs and TACs of the quantum dot are presented as a function of the incident photon energy. In addition, linear and non-linear contributions that only belong to the intermediate I-value are presented to avoid visual and logical

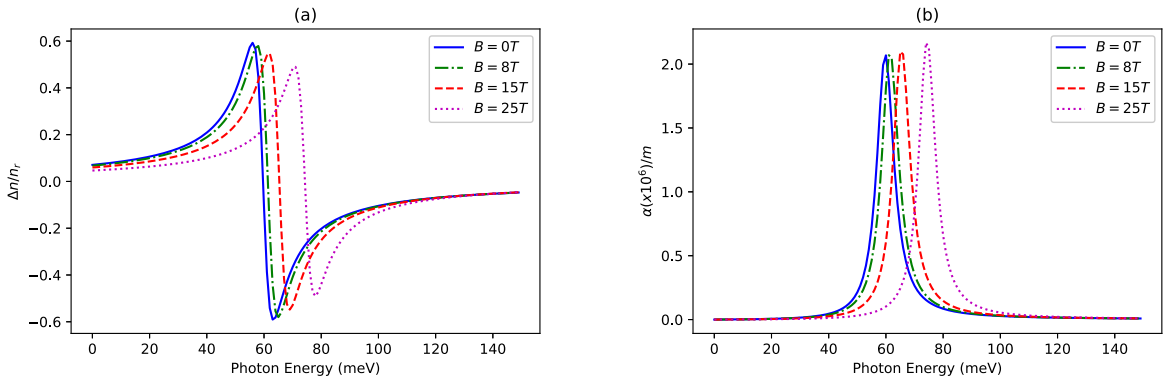

Fig. 6. (a) The TRICs and (b) TACs of the Mathieu quantum dot with $V_0 = 215.29$ meV ($x = 0.25$) and $\eta = 0.35/a_0$, under the influence of the external electric ($F = 5$ kV/cm) and magnetic field ($B = 1 - 8 - 15 - 25$ T), as a function of the incident photon energy.

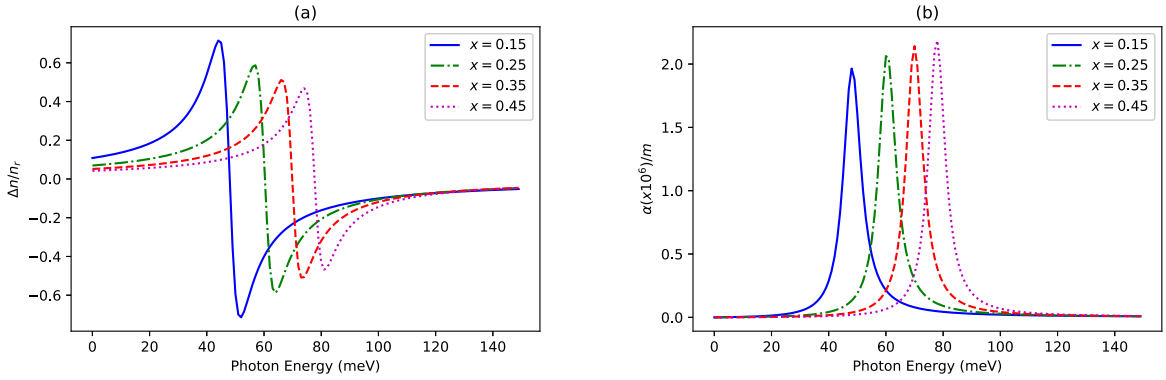

Fig. 7. When $\sigma_v = 6 \times 10^{23}$ m^{-3} and $I = 0.1 \times 10^{10}$ W/m^2, (a) the TRICs and (b) TACs of the Mathieu quantum dot with $x = 0.15 - 0.25 - 0.35 - 0.45$ and $\eta = 0.35/a_0$, under the influence of the external electric ($F = 5$ kV/cm) and magnetic field ($B = 5$ T), as a function of the incident photon energy.

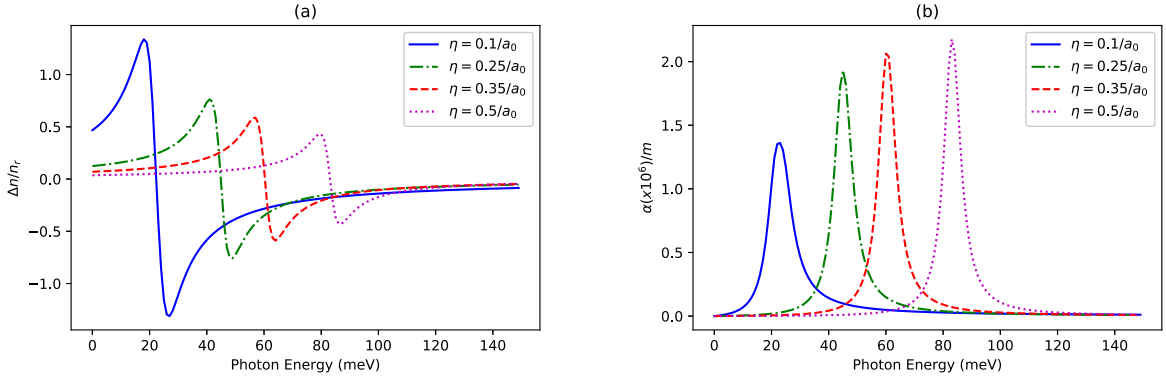

Fig. 8. (a) The TRICs and (b) TACs of the Mathieu quantum dot with $V_0 = 215.29$ meV ($x = 0.25$) and $\eta = 0.1 - 0.25 - 0.35 - 0.5a_0^{-1}$, under the influence of the external electric ($F = 5$ kV/cm) and magnetic field ($B = 5$ T), as a function of the incident photon energy.

confusion. As can be seen in Fig. 4, the increment of optical intensity within certain limits does not cause instability in the system. More precisely, the augment of optical intensity for out of appropriate limits can create an instability in the TRICs and TACs character of the quantum dot. That is, more peaks may constitute instead of two blatant resonance peaks in TRICs and one blatant resonance peak in TACs. This is because the quantum dot is subject to structural distortions due to exposition to high optical intensity. These strange features observed in the characteristics of TRICs and TACs, resulting from structural defects due to high I, determine the optimal I limit for TRICs and TACs. As can be seen, under the conditions in Fig. 4, the TACs of the Mathieu quantum dot become unstable in $I = 0.45 \times 10^{10}$ W/m^2, while its TRICs become unstable around $I = 0.8 \times 10^{10}$ W/m^2. In a nutshell, during the computations in the present study, the mentioned limits for the optimal range of the optical intensity should be taken into consideration. The increment of I leads to decrease the amplitudes, while it has no effect on resonant frequencies.

Fig. 5 presents the TRICs and TACs characters for different electric field strengths as a function of incident photon energy. As seen in Fig. 5a, the increase of F forms a blueshift in the TRICs resonant frequencies. Because, as can be clearly seen in Fig. 1a, as the electric field applied in the growth direction increases, the repulsion of the effective potential increases which in turn leads to a narrower potential profile at the left side of the structure. This repulsiveness causes also an augmentation in the trapping effect of the carriers. Then, the distance between the bound state energies formed in this new potential increases, which is the reason of the blueshift in TRICs resonant frequencies (See Fig. 2a and Fig. 5a). Similarly, as the external electric

field strength increases, the TRICs amplitudes decrease because of the decrement in the matrix elements ($|M_{fi}|^2$) (See Fig. 3a). However, the TACs are similar character to TRICs except for their amplitude behavior. As seen in Fig. 5b, the TACs resonant frequencies exhibit a blueshift due to the role of the electric field on the effective potential, as the same in the TRICs ones. However, the following situation is remarkable; the increment of the external electric field strength creates a rather monotonous effect on the TACs amplitudes. The reason of this monotonic effect is the physical result arising from the mathematics of the nonlinear effect as well as the monotony of the change in the matrix elements (See Fig. 5b and Fig. 3a).

The effects of the external magnetic field on the TRICs and TACs of the Mathieu quantum dot are shown in Fig. 6. In Fig. 6a, as the magnetic field increases, a blue shift is observed in the TRICs and TACs resonant frequencies. The repulsion of the effective potential increases with the increasing magnetic field (See Fig. 1b), as in the electric field effect. Because this shifting causes an enhancement in the gaps between the respective energy levels, a blue shift is observed in the optical resonant frequencies (See Fig. 6a, 6b). Also, increasing magnetic field causes a decrease in TRICs amplitudes as the increase in the magnetic field decreases the matrix elements (See Fig. 6a and Fig. 3b). When considering the TACs characters, the behavior of the TACs amplitudes is different. As seen in Fig. 6b, the increment of the external magnetic field causes an increase in the TACs amplitudes. Although the same behavior of the matrix elements in the changing B, the reason for such a different behavior compared to the behavior of TRICs amplitudes is the dominance of the third-order nonlinear contribution on the TACs, according to Eq. (18) (See Fig. 3b).

Fig. 7 shows the effect of potential depth of the Mathieu quantum dot on the TRICs and TACs as a function of incident photon energy. It can be seen in Fig. 7a that the increment of the potential depth (x) leads to blue shift in the TRICs resonant frequencies. The blueshift of the resonant peaks is due to the fact that the increased potential depth arising from In concentration (x) results in an increase in the difference between the energy levels (See Fig. 1c and Fig. 2c). The reason of the lowering in the TRICs amplitudes because of the increase of potential depth is that the matrix elements decreases as x increases, as can be seen in Fig. 3c. Fig. 7b introduces the TACs of the Mathieu quantum dot versus the different values of In−concentration as a function of the incident photon energy. The increase of x deepens the potential profile and increases the difference between the relevant energy levels, as can be seen in Fig. 1c and Fig. 2c, in which result affects on the TACs resonant frequencies and the relevant operation ends in a blue shift in TACs resonant frequencies. As seen in Fig. 7b, as mentioned earlier in a similar way, the augment of the In−concentration increases the TACs amplitudes in contrast to the behavior of TRICs amplitudes. Although the increase of the In-concentration decreases the matrix elements, the enhancement of the TACs amplitudes is due to the mathematical dominance between the linear-nonlinear contribution in ACs.

Fig. 8 shows the behavior of the TRICs and TACs for different values of the η parameter as a function of incident photon energy. Fig. 8a shows the effect of η on the TRICs. Since the increment of η increases the confinement effect, the respective energy gaps increase and then a blue shift in the TRICs resonant frequencies forms drastically (See Fig. 1d, Fig. 2d and Fig. 8a). In addition, increasing η decreases the TRICs amplitudes due to decreasing the matrix elements, as can be confirmed by considering Fig. 8a and Fig. 3d. As seen in Fig. 8b, the TACs resonant frequencies display a blueshift as a result of increasing η. It is important to note that the blue-shifting factors in the TRICs operate in the TACs. However, as with the other three parameters, the behavior of resonant amplitudes for the TACs is the opposite of the TRICs here too. As can be seen in Fig. 8b, the increment of the η parameter increases the amplitudes of the TACs, moreover, most strongly compared to the other three parameters. The reason for this case is related to the superiority of the linear and nonlinear contributions of the absorption coefficients to each other.

4. Conclusion

In the present work, the quantum dot with the Mathieu potential confinement, formed by the $In_xGa_{1-x}As/GaAs$ heterostructure, under the influence of the external electric and magnetic fields, has been considered. In this theoretical study, as well as the external field effects, the effects of structural parameters such as In-concentration and quantum dot width have been examined. In this manner, the effects of F, B, η and x parameters on the TRICs and TACs have been probed. The important results of the work can be highlighted as follows: (i) The usability of the electric and magnetic fields for the purpose is an important advantage, as they are external influences. Both external fields blueshift the resonant frequencies of the TRICs and TACs of the Mathieu quantum dot. In this respect, the external electric and magnetic field can be alternative to each other. The increment of these external fields reduces the TRICs amplitudes, so these external fields can also be an important argument in the optimization of the quantum dot for the TRICs. However, the external electric and magnetic field has almost no effect on the TACs amplitudes. (ii) As in the external fields, increasing the In−concentration is the reason of the blueshift in the resonant frequencies of the TRICs and TACs. The augment of this concentration decreases the TRICs amplitudes while increasing the TACs amplitudes. Therefore, the concentration increase has adverse effects on the optimality of the structure in terms of the TRICs and TACs. It should be emphasized that the concentration increase is more functional on the optimality of the TRICs character compared to that of the TACs. In addition, the following is an important point to be mentioned that as the concentration increase is an alternative to external fields in terms of resonant frequencies, it is also an alternative to external magnetic field in terms of character optimum. (iii) Increasing the width parameter of the Mathieu quantum dot leads to blueshift of the TRICs and TACs resonant frequencies, as in the other three effects. However, increasing the width parameter of the quantum dot decreases the TRICs amplitudes while increasing the TACs amplitudes. The important point here is that how to set the optimality of the dot width parameter in the consideration of the TRICs and TACs characters has been determined. (iv) When considering the characters of the TRICs and TACs, it is clear that the most dominant effect is the quantum dot width, followed by the concentration. In this manner, there is the predominance of structural parameters. However, the practicality of the external fields can also be evaluated as an advantage. (v) The values of the structure parameters and external fields given in the present work are achievable physical values. In this respect, the determination of the limit values of the carrier density of the Mathieu quantum dot and the relevant incident optical intensity is also remarkable in terms of experimental applications. (vi) Throughout the study, the spatial boundary has been taken as $R_{dot} = 6a_0$. However, the considered theoretical model and employed computational method can also be easily used for arbitrary spatial constraints under reasonable physical conditions. Since the Mathieu quantum dot is a periodically repeating potential at larger spatial boundaries, it can also be used in the application areas of multiple quantum wells, which is an advantage that can be considered in terms of the functionality of the Mathieu quantum dot. This work can be evaluated as a manual of the Mathieu quantum dot, which is considered for the first time in the related literature, which in turn this manuel also contains remarkable informations for both theoretical and experimental research.

CRediT authorship contribution statement

P. Başer: Conception and design of study, Acquisition of data, Analysis and/or interpretation of data, Writing - original draft, Writing - review & editing. **M.K. Bahar:** Conception and design of study, Acquisition of data, Analysis and/or interpretation of data, Writing - original draft, Writing - review & editing.

Declaration of competing interest

The authors declare that they have no known competing financial interests or personal relationships that could have appeared to influence the work reported in this paper.

Acknowledgment

All authors approved the version of the manuscript to be published.

References

[1] A.J. Nozik, Quantum dot solar cells, Phys. E 14 (2002) 115.
[2] R.D. Schaller, V.I. Klimov, High efficiency carrier multiplication in PbSe nanocrystals: Implications for solar energy conversion, Phys. Rev. Lett. 92 (2004) 186601.
[3] A.J. Nozik, M.C. Beard, J.M. Luther, M. Law, R.J. Ellingson, J.C. Johnson, Semiconductor quantum dots and quantum dot arrays and applications of multiple exciton generation to third-generation photovoltaic solar cells, Chem. Rev. 110 (2010) 6873.
[4] S. Fafard, K. Hinzer, S. Raymond, M. Dion, J. McCaffrey, Y. Feng, S. Charbonneau, Red-emitting semiconductor quantum dot lasers, Science 274 (1996) 1350.
[5] N. Kirstaedter, N.N. Ledentsov, M. Grundmann, D. Bimberg, V.M. Ustinov, S.S. Ruvimov, M.V. Maximov, P.S. Kopev, Zh. I. Alferov, U. Richter, P. Werner, U. Gösele, J. Heydenreich, Low threshold, large to injection laser emission from (InGa) as quantum dots, Electron. Lett. 30 (1994) 1416.
[6] G. Konstantatos, I. Howard, A. Fischer, S. Hoogland, J. Clifford, E. Klem, L. Levina, E.H. Sargent, Ultrasensitive solution-cast quantum dot photodetectors, Nature 442 (2006) 180.
[7] S.A. McDonald, G. Konstantatos, S. Zhang, P.W. Cyr, E.J.D. Klem, L. Levina, E.H. Sargent, Solution processed PbS quantum dot infrared photodetectors and photovoltaics, Nature Mater. 4 (2005) 138.
[8] G. Konstantatos, E.H. Sargent, Solution-processed quantum dot photodetectors, Proc. IEEE 97 (2009) 1666.
[9] J. Phillips, K. Kamath, P. Bhattacharya, Far-infrared photoconductivity in self-organized InAs quantum dots, Appl. Phys. Lett. 72 (1998) 2020.
[10] C. Hu, D. Dong, X. Yang, K. Qiao, D. Yang, H. Deng, S. Yuan, J. Khan, Y. Lan, H. Song, J. Tang, Synergistic effect of hybrid PbS quantum dots/2D-WSe 2 toward high performance and broadband phototransistors, Adv. Funct. Mater. 27 (2017) 1603605.
[11] K.S. Cho, E.K. Lee, W.-J. Joo, E. Jang, T.-H. Kim, S.J. Lee, S.-J. Kwon, J.Y. Han, B.-K. Kim, B.L. Choi, J.M. Kim, High-performance crosslinked colloidal quantum-dot light-emitting diodes, Nat. Photon. 3 (2009) 341.
[12] L. Qian, Y. Zheng, J. Xue, P.H. Holloway, Stable and efficient quantum-dot light-emitting diodes based on solution-processed multilayer structures, Nat. Photon. 5 (2011) 543.
[13] K.H. Lee, J.-H. Lee, W.-S. Song, H. Ko, C. Lee, J.-H. Lee, H. Yang, Highly efficient, color-pure, color-stable blue quantum dot light-emitting devices, ACS Nano 7 (2013) 7295.
[14] I. Lagraa, B. Soudini, H. Abid, S. Taleb, Study and optimization of structure InAs/InGaAs quantum dot in-a-well long-wave infrared photodetector, Optik 251 (2022) 168494.
[15] M. Felle, J. Huwer, R.M. Stevenson, J. Skiba-Szymanska, M.B. Ward, I. Farrer, R.V. Penty, D.A. Ritchie, A.J. Shields, Interference with a quantum dot single-photon source and a laser at telecom wavelength, Appl. Phys. Lett. 107 (2015) 131106.
[16] R. Benchamekh, S. Schulz, E.P. O'Reilly, Theoretical analysis of influence of random alloy fluctuations on the optoelectronic properties of site-controlled (111)-oriented InGaAs/GaAs quantum dots, Phys. Rev. B 94 (2016) 125308.
[17] R. Singh, G. Bester, Nanowire quantum dots as an ideal source of entangled photon pairs, Phys. Rev. Lett. 103 (2009) 063601.
[18] G.C. Osburn, $In_xGa_1 - xAsIn_yGa_1 - y$As strained-layer superlattices: A proposal for useful, new electronic materials, Phys. Rev. B 27 (1983) 5126.
[19] P. Bhattacharya, S. Ghosh, A.D. Stiff-Roberts, Annu. Rev. Mater. Res. 34 (2004) 1.
[20] V. Vadim, Quantum dot infrared photodetectors: Interdot coupling, J. Appl. Phys. 100 (2006) 076101.
[21] M. Luisier, N. Neophytou, N. Kharche, G. Klimeck, Full-band and atomistic simulation of realistic 40 nm InAs HEMT, in: IEEE International Electron Devices Meeting, Vol. 1, 2008, p. 4.
[22] P. Blood, E.D. Fletcher, K. Woodbridge, Strained layer GaInAs/GaAs 1um wavelength quantum well lasers, in: Presented At the IOP Solid, 1989.
[23] Y.A. Goldberg, N.M. Shmidt, Gallium Indium Arsenide, in: M. Levinshtein, S. Rumayantsev, M.S. Shur (Eds.), Handbook Series on Semiconductor Parameters, Vol. 2, World Scientific, Singapore, 1999, p. 62.
[24] T.P. Pearsall, R.W. Hopson Jr., Electronic materials conference, Cornell University, 1977 Publ, J. Electron. Mat. 7 (1978) 133.
[25] A.V. Thathachary, N. Agrawal, L. Liu, S. Datta, Electron transport in multi-gate $In_xGa_{1-x}As$ nanowire FETs: from diffusive to ballistic regimes at room temperature, Nano Lett. 14 (2014) 626.
[26] J.D. Dow, D. Redfield, Electroabsorption in semiconductors: The excitonic absorption edge, Phys. Rev. 8 (1970) 3358.
[27] Q.H.F. Vrehen, Interband magneto-optical absorption in gallium arsenide, J. Phys. Chem. Solids 29 (1968) 129.
[28] R. Dingle, W. Wiegmann, C.H. Henry, Quantum states of confined carriers in very thin $Al_xga_{1-x}As$-GaAs-$Al_xGa_{1-x}As$ heterostructures, Phys. Rev. Lett. 33 (1974) 827.
[29] D.A.B. Miller, D.S. Chemla, T.C. Damen, A.C. Gossard, W. Wiegmann, T.H. Wood, C.A. Burrus, Band-edge electro absorption in quantum well structures: The quantum-confined stark effect, Phys. Rev. Lett. 53 (1984) 2173.
[30] E.J. Austin, M. Jaros, Electronic structure of an isolated GaAs-GaAlAs quantum well in a strong electric field, Phys. Rev. B 31 (1985) 5569.
[31] E.S. Moskalenko, M. Larsson, W.V. Schoenfeld, P.M. Petroff, P.O. Holtz, Carrier transport in self-organized InAs-GaAs quantum-dot structures studied by single-dot spectroscopy, Phys. Rev. B 73 (2006) 155336.
[32] A. Larsson, Optical Spectroscopy of InGaAs Quantum Dots, Linköping University Electronic Press, 2011.
[33] V.V. Fock, Bemerkung zur Quantelung des harmonischen oszillators im magnetfeld, Physica A 47 (1928) 446.
[34] T. Tanaka, Y. Arakawa, G.W.E. Bauer, Magnetoexcitons in quantum wires with an anisotropic parabolic potential, Phys. Rev. B 50 (1994) 7719.
[35] S. Raymond, S. Studenikin, A. Sachrajda, Z. Wasilewski, S.J. Cheng, W. Sheng, P. Hawrylak, A. Babinski, M. Potemski, G. Ortner, M. Bayer, Excitonic energy shell structure of self-assembled InGaAs/GaAs quantum dots, Phys. Rev. Lett. 92 (1994) 187402.
[36] Z.H. Zhang, K.X. Guo, B. Chen, R.-Z. Wang, M.-W. Kang, S. Shao, Theoretical studies on the optical absorption coefficients and refractive index changes in parabolic quantum dots in the presence of electric and magnetic fields, Superlattices Microstruct. 47 (2010) 325.
[37] M. Gambhir, V. Prasad, Dependence of nonlinear optical properties on electrostatic interaction in an excitonic parabolic quantum dot in a static magnetic field, J. Modern Opt. 68 (2021) 542.
[38] T.A. Sargsian, M.A. Mkrtchyan, H.A. Sarkisyan, D.B. Hayrapetyan, Effects of external electric and magnetic fields on the linear and nonlinear optical properties of InAs cylindrical quantum dot with modified Pöschl-Teller and Morse confinement potentials, Physica E 126 (2021) 114440.
[39] S.L. Talwar, S. Lumb, V. Prasad, Optical properties of hydrogenic impurity in a distorted quantum disk, Eur. Phys. J. Plus 137 (2022) 175.
[40] D. Makhlouf, M. Choubani, F. Saidi, H. Maaref, Modeling of the second harmonic generation in a lens-shaped InAs/GaAs quantum core/shell dot under temperature, pressure and applied electric field effects, Results Phys. 16 (2020) 102961.
[41] R. Khordad, Third-harmonic generation in a double ring-shaped quantum dot under electron–phonon interaction, Opt. Commun. 391 (2017) 121.
[42] S. Evangelou, Nonlinear optical rectification of a coupled semiconductor quantum dot – Metallic nanosphere system under a strong electromagnetic field, Physica B 556 (2019) 170.
[43] J. Meixner, F.W. Schafke, Mathieusche Funktionen Und Spharoidfunktionen, Springer, Berlin, 1954.
[44] H.H. Aly, H.J.W. Müller-Kirsten, N. Vahedi-Faridi, Scattering by singular potentials with a perturbation-theoretical introduction to Mathieu functions, J. Math. Phys. 16 (1975) 961.
[45] G. Torres-Vega, J.D. Morales-Guzman, A. Zuniga-Segundo, Special functions in phase space: Mathieu functions, J. Phys. A: Math. Gen. 31 (1998) 6725.
[46] M. Kalinski, J.H. Eberly, New states of hydrogen in a circularly polarized electromagnetic field, Phys. Rev. Lett. 77 (1996) 2420.
[47] G.-H. Sun, C.-Y. Chen, H. Taud, C. Yanez-Marquez, S.-H. Dong, Phys. Lett. A 384 (2020) 126480.
[48] S. Adachi, GaAs, AlAs, and AlxGa1xAs: Material parameters for use in research and device applications, J. Appl. Phys. 58 (1985) R1.
[49] P. Harrison, Quantum Wells, Wires, Dots, second ed., Wiley, UK, 2005.
[50] B.N. Datta, Numerical Linear Algebra and Applications, second ed., Mdpi, USA, 2010.
[51] R.W. Boyd, Nonlinear Optics, third ed., Rochester, New York, 2007.
[52] D. Ahn, S. Chuang, IEEE J. Quantum Electron. 23 (12) (1987) 2196.